Reference Particles for Toxicological Studies of Wood Combustion: Formation, Characteristics, and Toxicity Compared to Those of Real Wood Combustion Particulate Mass

ARTICLE *in* CHEMICAL RESEARCH IN TOXICOLOGY · JULY 2014

Impact Factor: 3.53 · DOI: 10.1021/tx500142f · Source: PubMed

9 AUTHORS, INCLUDING:

Oskari Juuso Uski
University of Eastern Finland
14 PUBLICATIONS **131** CITATIONS
SEE PROFILE

Pasi I Jalava
University of Eastern Finland
50 PUBLICATIONS **955** CITATIONS
SEE PROFILE

Olli Sippula
University of Eastern Finland
66 PUBLICATIONS **592** CITATIONS
SEE PROFILE

Maija-Riitta Hirvonen
University of Eastern Finland
167 PUBLICATIONS **3,272** CITATIONS
SEE PROFILE

Chemical Research in Toxicology

Article

pubs.acs.org/crt

Reference Particles for Toxicological Studies of Wood Combustion: Formation, Characteristics, and Toxicity Compared to Those of Real Wood Combustion Particulate Mass

Tiina Torvela,*[,†] Oskari Uski,[†,‡] Tommi Karhunen,[†] Anna Lähde,[†] Pasi Jalava,[†,‡] Olli Sippula,[†] Jarkko Tissari,[†] Maija-Riitta Hirvonen,[†,‡] and Jorma Jokiniemi[†,§]

[†]Department of Environmental Science, University of Eastern Finland, P.O. Box 1627, FI-70211 Kuopio, Finland

[‡]Department of Environmental Health, National Institute for Health and Welfare, P.O. Box 95, FI-70701 Kuopio, Finland

[§]VTT Technical Research Centre of Finland, P.O. Box 1000, FI-02044 VTT Espoo, Finland

ABSTRACT: Multiple studies show that particulate mass (PM) generated from incomplete wood combustion may induce adverse health issues in humans. Previous findings have shown that also the PM from efficient wood combustion may induce enhanced production of reactive oxygen species (ROS), inflammation, and cytotoxicity *in vitro* and *in vivo*. Underlying factors of these effects may be traced back to volatile inorganic transition metals, especially zinc, which can be enriched in the ultrafine fraction of biomass combustion particulate emission. In this study, nanoparticles composed of potassium, sulfur, and zinc, which are the major components forming inorganic fine PM, were synthesized and tested *in vitro*. In addition, *in vitro* toxicity of PM from efficient combustion of wood chips was compared with that of the synthesized particles. Cytotoxicity, cell cycle arrest, ROS generation, and tumor necrosis factor alpha release were related to zinc concentration in PM. Potassium sulfate and potassium carbonate did not induce toxic responses. In light of the provided data, it can be concluded that zinc, enriched in wood combustion emissions, caused the toxicity in all of the measured end points.

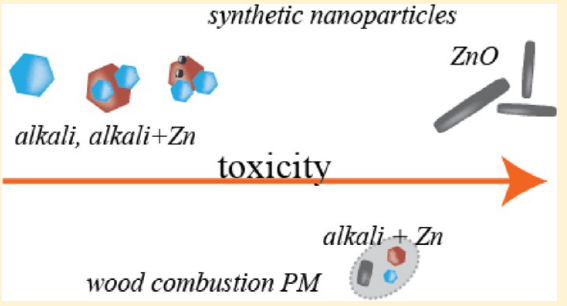

INTRODUCTION

Airborne particulate mass (PM) is known to cause adverse health effects in humans, including respiratory and cardiovascular diseases.[1,2] Residential biomass combustion is recognized as being one of the most important sources of fine particulate mass (particles ≤2.5 μm in aerodynamic diameter, $PM_{2.5}$) in urban environments.[3] In addition, the political decisions to increase biomass combustion in small scale local systems may increase the emissions of fine and ultrafine particles (UFPs, aerodynamic diameter ≤100 nm) in the future. According to epidemiological studies,[4] not only elemental and organic carbon (EC and OC) but also various transition metals such as cadmium and zinc (Zn) are associated with mortality. In efficiently operated modern appliances, e.g., pellet boilers, the particle emissions are dominated by inorganic ash species, whereas the incomplete combustion conditions produce particles which mostly consist of EC and OC.[5]

The particle physical properties such as size, surface area, morphology, number concentration, chemical composition, and solubility play an important role when assessing the health effects of particles.[6,7] The aerodynamic diameter of wood combustion particles is mostly smaller than 1 μm (PM_1).[8] Because of the small size, these particles can be deposited in the tracheobronchial and alveolar regions of the respiratory track, whereas larger particles ($PM_{10-2.5}$ and $PM_{2.5-1}$) are deposited in the extrathoracic region of the airways.[9] In particular, the UFPs are believed to be potentially dangerous due to their small size, large surface area to mass ratio, deep airway penetration, and ability to be retained in the lung; they may even penetrate through the lung tissue and reach the capillary blood vessels and circulating cells.[6] They also contain a high content of redox-cycling organic and inorganic compounds.[10] Thus, the chemical composition associated with the PM is most important for the smallest PM size fractions. Indeed, UFPs have their own specific linkage on cardiovascular morbidity.[11,12]

The typical fine particles formed in efficient wood combustion contain mainly potassium, sulfur, chlorine, and zinc (K, S, Cl, and Zn).[13,14] These volatile components are released in the high temperature flame and subsequently form particles by nucleation and condensation as the flue gas cools down. Recently, we have published *in vivo* and *in vitro* data suggesting the possibly significant role of Zn in the toxicity of PM emissions from residential wood combustion.[15−17] Previously, it has been observed that zinc, as a divalent Zn^{2+} ion, is able to induce necrotic cell death in human bronchial epithelial cells (BEAS-2) as well as RAW264.7 macrophages.[18] Moreover, significant increase in lactate dehydrogenase (LDH) and total protein has been reported in mice intratracheally exposed to zinc chloride.[19] Zn^{2+} cytotoxicity is shown to be

Received: April 17, 2014

   dx.doi.org/10.1021/tx500142f | *Chem. Res. Toxicol.* XXXX, XXX, XXX−XXX

Table 1. Precursor Solution Compositions Used in Flame Spray Pyrolysis Particle Synthesis

precursor solute formula concn	K-acetylcetonate $C_5H_7O_2K$ (mmol L^{-1})	dimethyl sulfoxide C_2H_6OS (mmol L^{-1})	Zn-acetate dihydrate $C_4H_{10}O_6Zn{\cdot}2H_2O$ (mmol L^{-1})
Zn	[-]	[-]	30
K/S/Zn	20	80	0.6
K/S	20	80	[-]
K	100	[-]	[-]

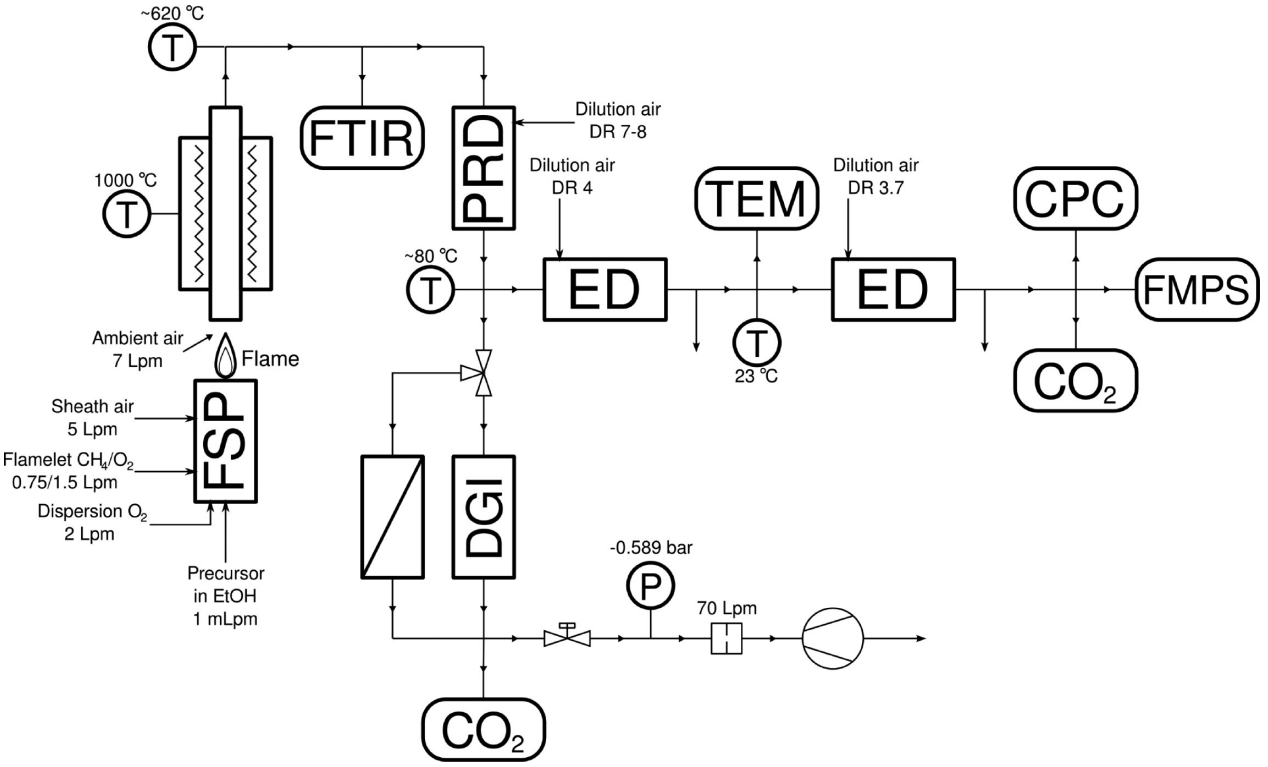

Figure 1. Experimental setup of FSP for nanoparticle synthesis including the high temperature furnace and sampling sections. Nomenclature: T = temperature sensor, P = pressure sensor, CO_2 = CO_2 sensor, PRD = porous tube diluter, ED = ejector diluter, DGI = Dekati gravimetric impactor, TEM = sampling for transmission electron microscopy, CPC = condensation particle counter, FMPS = fast mobility particle sizer, and DR = dilution ratio.

linked to ROS production inside the cell.[20] In addition to zinc ions, it has been shown *in vitro* that ZnO particles may induce cytotoxicity in human lung epithelial cells.[21,22]

In addition, a link between ambient sulfate concentrations and long-term effects on mortality has been seen in epidemiological studies (e.g., Elliott et al.[23] and Willis et al.[24]). Other reports, e.g., by Abrahamowicz et al.,[25] have challenged the relationship: it is suggested that the sulfates may act more as a surrogate for other pollutants associated with them.[26] Therefore, the constitute-specific role of sulfate, as well as potassium alone, remains unclear. Sulfates mostly derive secondarily from oxidation of sulfur dioxide SO_2.[27] In PM samples collected from various urban sites, secondary sulfate has not been associated with significant toxicological effects.[28,29]

On the basis of recent results, wood combustion conditions and chemical composition of the emission particles have strong effects on the induced toxicological responses in immunological cells *in vitro*.[30−33] However, showing a direct connection between a toxic agent and clinical toxicity is not straightforward due to the complexity of ambient PM. Toxicity screening has been successfully carried out using engineered nanomaterials. At the cellular level, converging features for both ambient PM and engineered nanomaterial toxicity do exist.[34,35] In this study, nanoparticles that were compositional simplifications of particles formed during wood combustion were synthesized, characterized, and tested *in vitro*, and compared with the data previously published for combustion PM. The main focus of this study was to investigate the effects of alkali salts and zinc on the toxicity of PM. For nanomaterial production, flame spray pyrolysis (FSP) was adopted due to the simplicity of use, purity of end-products, and adjustability of the method.[36] It is also a widely used method in the production of metal oxides for toxicity screening studies.

MATERIALS AND METHODS

Particle Production. *Synthetic Particles.* Composite particles containing potassium, sulfate, and zinc were generated using FSP.[36] The used precursor components were potassium acetylacetonate ($C_5H_7O_2K$), dimethyl sulfoxide (C_2H_6OS), and zinc acetate dihydrate ($C_4H_{10}O_6Zn{\cdot}2H_2O$), all from Sigma-Aldrich. The precursor components were dissolved in ethanol (Etax Aa 99.5%, Altia, Finland) as shown in Table 1. The studied cases are denoted as "K" "K/S", "K/S/Z", and "Zn". The ratio of potassium to zinc was chosen to correspond to the compositions observed in emissions from wood-fired combustion plants.[37] However, a clear excess of sulfur was provided

dx.doi.org/10.1021/tx500142f | Chem. Res. Toxicol. XXXX, XXX, XXX−XXX

Table 2. Gaseous Concentrations of the Combustion Gases and Water (Dry, at 17% O_2 Concentration), the Calculated Dilution Ratios of the PRD, and the Calculated Input Volumetric Flow Rate of the Reaction Gases after the Flame[a]

	dilution ratio PRD	flow rate (1 min^{-1})	H_2O FTIR (vol %)	O_2 (vol %)	CO (ppm)	SO_2 (ppm)	NO_x (ppm)	$CO_2 \times 10^4$ (ppm)
K	6.8	17.0	14.4	17.3	32	<10	390	1.75
Zn	6.8	17.0	14.0	17.5	<10	140	350	1.71
K/S/Zn	6.9	17.1	15.0	17.2	<10	110	300	1.73
K/S	7.6	17.1	14.8	17.5	<10	<10	400	1.71

[a]The concentration of CO_2 is from a point after the DGI.

for the process in order to ensure the high sulfation rate of the potassium species.

The material precursors dissolved in ethanol were dispersed by oxygen gas and ignited. Within the resulting high-temperature, high-oxygen content flame, the precursors underwent complete dissociation, oxidation, and subsequent nucleation. Efficient cooling of the process gas ensured rapid quenching, thereby reducing particle sintering.

The setup used is shown in Figure 1. The precursors were fed at a constant rate of 1 mL min^{-1}. Pure oxygen was used as dispersion gas for the precursor liquid and as an oxidant in combustion at a flow rate of 2 L min^{-1}. A flamelet of premixed methane and oxygen in stoichiometric ratio was used to ignite and maintain the main flame. A flow rate of 5 L min^{-1} of particle free, dry sheath air was added before the flow reactor inlet, in order to minimize losses in the reactor walls. In addition, a certain volume of laboratory air entered the system at the flame junction, which was in contact with the ambient air. The volume of the laboratory air was determined by calculating the stoichiometric combustion products and balancing them to correspond to the measured concentrations of CO_2, H_2O, and O_2. Hence, a constant flow rate of 7 L min^{-1} of laboratory air was determined. The combustion products were fed into a 80 cm long silicon carbide flow reactor tube (inner diameter 28 mm) heated to a 1000 °C. This provides a sufficient temperature and residence time for the sulfation reactions of the potassium vapors, as was recently shown by Sippula et al.[27] in a similar flow reactor setup.

Combustion Particles. As a reference for the synthetic composite particles, PM_1 from the combustion of commercial wood chips was also collected for *in vitro* testing. The particles were produced using an efficient combustion setting (CO emission below 100 mg MJ^{-1} and PM_1 emission below 10 mg MJ^{-1}) in a 40 kW combustion unit, the operation and emissions of which has been described in detail by Leskinen et al.[14]

Sampling and Characterization of Generated Aerosols. *Dilution Procedure.* The dilution of the particle samples were carried out in three stages, using a porous tube diluter (PRD) and two ejector type diluters (ED) in series (Figure 1). The dilution system has been well characterized in several biomass combustion studies.[14,32,38−40] Filtered, dry air at room temperature was used for the dilution, and the dilution flow rates were controlled with mass flow controllers. The dilution ratio (DR) in the first dilution section, directly after the exit of the heated zone of the reactor, varied between approximately 7 and 8 (Table 2). It was determined using the carbon dioxide (CO_2) concentrations, measured before and after the first dilution section (eq 1) as follows:

$$\frac{CO_{2,u} - CO_{2,b}}{CO_{2,d} - CO_{2,b}} \quad (1)$$

where $CO_{2,u}$ and $CO_{2,d}$ are the undiluted and diluted CO_2 concentrations, and $CO_{2,b}$ is the CO_2 concentration of the dilution air. The DRs in the second and third dilution stages were 4 and 3.7, respectively, according to the inlet and sampling air flow rates measured for the ejector diluters.

Gaseous Composition. A Fourier transform infrared analyzer (FTIR, Gasmet Technologies Inc., Finland) was used to measure concentrations of carbon monoxide (CO), carbon dioxide, sulfur dioxide (SO_2), water, and a number of other gaseous compounds. The emission concentrations measured using the FTIR were either normalized to 17% oxygen concentration in the dry flue gas or presented as concentration per unit volume. The O_2 concentration of 17% was chosen for the normalization because the measured concentration was near that value during all of the experiments.

Particle Concentrations. The number size distribution of FSP generated particles was determined using a fast mobility particle sizer (FMPS 3091, TSI Inc., USA), and the number concentration using a condensation particle counter (CPC 3775, TSI Inc., USA). The concentrations were corrected using the determined dilution ratios. Presented values were calculated as an average of scans during particulate sample collection for the chemical and toxicological analyses.

Collection of Particulate Mass. PM_1 samples for the toxicological and chemical analyses were collected on polytetrafluoroethylene (PTFE) substrates after the first dilution stage (PRD, Figure 1) with a Dekati gravimetric impactor (DGI, Dekati Ltd., Finland), using a previously validated method.[41] The handling of the sampling substrates prior to collection and the PM sample preparation was carried out by the method validated by Jalava et al.[42] Briefly, particulate mass collected on filters at DGI stages $PM_{1-0.5}$, $PM_{0.5-0.2}$ and the filter stage $PM_{0.2}$ were prepared as follows. The filters were cut in pieces and eluted with methanol in an ultrasonic water bath (FinnSonic m20, FinnSonic Ltd., Finland) 2 × 30 min below +35 °C. The suspensions from each setup were pooled to form a PM_1. Excess methanol from suspensions was evaporated at +35 °C and 150 mbar in a rotary evaporator (Heidolph Instruments GmbH & Co. KG, Germany). Finally, for various chemical and toxicological analyses, the sample material was divided to gravimetrically determined aliquots, which were dried in glass tubes under nitrogen (99.5%) flow, and stored at −20 °C. Identical handling was done for the blank substrates used as control in the toxicological studies.

Determination of Elements and Anions. Mass of multiple elements (Ag, Al, As, B, Ba, Be, Bi, Ca, Cd, Co, Cr, Cu, Fe, K, Li, Mg, Mn, Mo, Na, Ni, Pb, Rb, Sb, Se, Si, Sr, Th, Ti, Tl, U, V, and Zn) and anions (Cl^-, Br^-, F^-, NO^{3-}, SO_4^{2-}, and PO_4^{3-}) were determined from the PM_1 samples. Samples for element analysis were eluted with HF-HNO_3 acid and analyzed using an inductively coupled plasma mass spectrometer (ICP-MS, PerkinElmer Elan 6000). The samples for ion analysis were eluted with deionized water and analyzed using ion chromatography (IC, Dionex DX-120).

Crystalline Composition. X-ray diffraction (XRD) was performed on a Bruker D8 Discover (Cu Kα source, 40 kV, 40 mA) and analyzed with Bruker DIFFRAC.EVA software. The diffraction was measured for 2Θ angles of 5−70° and 10−70° with a step size of 0.05° and 0.03°. The integration time per step was 38.4 s for all samples. The domain sizes were calculated for each diffraction peak using the Scherrer equation.[43] By averaging these sizes for diffraction peaks corresponding to lattice directions parallel and perpendicular to the crystal growth direction [001], an estimate of the crystallite length and width was obtained. The ratio of these is then the crystal aspect ratio, while the length parameter is used as the crytallite size in subsequent analysis.

Particle Morphology. Samples for transmission electron microscopy (TEM) were collected on a carbon film with holes (S147-400 Holey Carbon Film 400 Mesh Cu, Agar Scientific, UK) using an aspiration sampler, consisting of a stainless steel tube (inner diameter 2.8 mm) with a grid holder and a vacuum pump adjusted with a needle valve to maintain an air flow of 0.3 cm^3 min^{-1} through the tube. The TEM and energy dispersive X-ray spectroscopy (EDS) analyses were

dx.doi.org/10.1021/tx500142f | Chem. Res. Toxicol. XXXX, XXX, XXX−XXX

carried out using a JEM 2100-F (JEOL Ltd., Japan) field emission TEM equipped with a Si(Li)-type detector coupled with an EDS analyzer system (NS7, Thermo Fisher Scientific Inc., USA). The microscope was operated at 200 kV acceleration voltage.

Study Design of Toxicological Analyses. Study design and methods for toxicological analyses are described in more detail elsewhere.[17,31] Mouse macrophage cells (RAW264.7, ATCC, USA) were grown in RPMI 1640 medium supplemented with 10% heat inactivated fetal bovine serum, 2 mM L-glutamine, and 100 U mL^{-1} penicillin−streptomycin in a humid atmosphere of 5% CO_2 (37 °C). On the day before the experiments, the cell suspension at a concentration of 5×10^5 cells mL^{-1} was dispensed into 6-well plates (2 mL/well, Corning Inc., USA). Fresh culture medium (2 mL/well) was changed 1 h before exposure of the cells to particles or their controls.

Half an hour before the exposure, emission particles were suspended into DMSO (20 μL mg^{-1}, Merck KGaA, Germany). After that, pathogen-free water (W1503, Sigma-Aldrich Corp., USA) was added to gain a PM concentration of 5 mg mL^{-1}. To suspend the particles, the sample was sonicated in an ultrasonic water bath (FinnSonic m03, FinnSonic Ltd., Finland) for 30 min below +35 °C. Mouse RAW264.7 macrophages were exposed for 24 h to four doses (15, 50, 150, and 300 μg mL^{-1}) of emission particles from each case. Corresponding DMSO concentrations were 4.2, 14.0, 41.1, and 84.2 μM, and H_2O concentrations were 0.2, 0.6, 1.7, and 3.3 mM in the exposure medium.

Exposures of the cells to the particulate samples were made in three independent experiments, which included the blank substrate (dose 150 μg mL^{-1}), water (dose 1.7 mM), and DMSO (dose 41.1 μM) control. After the 24 h exposure, the macrophages were scraped from the wells. The cell suspension was centrifuged (8000 G, 5 min, +4 °C) to separate the cells and particles from the cell culture medium. The supernatant was stored at −80 °C for the analysis of inflammatory mediators. The cells were suspended into 1 mL of PBS (Gibco, UK), and half of them were used in a propidium iodide exclusion assay, and the other half was fixed with ethanol (70% v/v, Altia, Finland) and stored at +4 °C for DNA content analysis with flow cytometry (CyAn ADP, Beckman Coulter Inc., USA). For ROS analysis, another PM exposure experiment was done as described by Uski et al.[17]

Flow Cytometry Analysis. Particle induced effects on cell cycle, total amount of propidium iodide (PI) positive cells (PI-exclusion assay), and the intracellular accumulation of reactive oxygen and nitrogen species were analyzed using a CyAn ADP (Beckman Coulter Inc., USA) cytometer with Summit software (version 4.3; Beckman Coulter Inc., USA). A total of 12000 cells per sample were analyzed.

Production of Inflammatory Mediator. The production of a proinflammatory cytokine, tumor necrosis factor alpha (TNF-α), was analyzed from cell culture medium using commercial ELISA kits (R&D Systems, USA). The analysis was performed according to the manufacturer's instructions.

Zinc Concentration. Because of their different origins, the zinc mass concentration varied between the samples. The calculated maximum free zinc ion concentrations (C_{MFZ}) of the samples corresponding to different particle mass based doses are listed in Table 3. The C_{MFZ} varied in the range 0−170 μg mL^{-1} corresponding to molar concentrations of approximately 0−2500 μM of Zn^{2+}. The C_{MFZ} of "K/S/Zn" ranged from 0.1−2.5 μg mL^{-1} (2−38 μM) and that of the "Zn" sample from 8.5−170 μg mL^{-1} (130−2600 μM) of Zn^{2+}. The zinc concentration of the wood chips (35 mg/kg) was a typical level for untreated wood fuels[44] and resulted in the C_{MFZ} of 0.9−17.4 μg mL^{-1} (13−270 μM) for PM_1 from the wood chip combustion.

Table 3. Correspondance of the Maximum Free Zinc Ion Concentration (C_{MFZ} (μg/mL)) of the Samples with the Particle Mass Doses

		particle mass based dose (μg mL^{-1})			
experiment		5	50	150	300
K		0.01	0.05	0.14	0.27
K/S		0.03	0.10	0.29	0.57
K/S/Zn	C_{MFZ} (μg mL^{-1})	0.13	0.42	1.26	2.52
wood PM		0.87	2.90	8.70	17.40
Zn		8.49	28.30	84.90	169.80

Calculations. *Combustion Products.* Stoichiometric composition of combustion gases was calculated in order to trace back the particle synthesis conditions in the flow reactor and to compute the thermodynamic equilibrium. The weight fractions of the elements C, H, O, S, K, and Zn were first determined from the precursor molar quantities by formula. The molar flow rates of the combustion gases were determined from the precursor and gas feed rates assuming complete combustion. Thus, CO_2, H_2O, and SO_2 were assumed to be formed from the combustible species. The flow rates of excess O_2 as well as the refractory cations K and Zn were added as nonreactive components. In addition, the sheath and laboratory air streams were added to the calculations as a two-component simple dry air mixture (79% N_2, 21% O_2). As a result, the estimated total combustion gas volumetric flow rates at the flow reactor tube were between 17.0 and 17.1 L min^{-1} (NTP).

To be comparable with each other, all measured and calculated gas volumes were corrected to dry volumes at normal temperature and pressure (NTP, 0 °C, 1 atm), and reduced to an oxygen concentration of 17%.

Thermodynamic Equilibrium. Particle formation in the flow reactor was interpreted by thermodynamic equilibrium calculations, using FactSage 6.3.[45] The computed molar flow rates of combustion gases were fractionated into input streams of O_2, N_2, CO_2, H_2O, SO_2, K, and Zn. Thermodynamic equilibrium among solid, liquid, and gaseous species in atmospheric pressure at temperatures between 1400 and 80 °C was calculated. Thermodynamic data were taken from the FactPS database of the software. Moreover, the thermodynamic values of gaseous zinc oxide, adopted from HSC Chemistry (Outotec Oy, Finland), were added to the solution database. The equilibrium calculations describe the particle formation during the cooling phase of the combustion gases after the flame. The reaction kinetics at high flame temperatures (2200−2600 K) are too fast to reach any equilibrium, which must be held in mind when interpreting the results. It must be noted also that in the FSP some oxidation reactions could take place already at the flame[46] as the flame is premixed with oxygen.

Statistical Analyses. The measured toxicological responses were compared to the control and corresponding blank samples with regard to particle doses. The data was statistically analyzed in IBM SPSS Statistics 19.0 (SPSS Inc., Chicago, IL, USA). Levene's test for equality of variances was used for all the samples before analyzing the data using analysis of variance (ANOVA). Dunnett's posthoc test was used when results from the production of TNF-α ($n = 6$) was analyzed. The results from the ROS analyses, PI-exclusion assay, and cell cycle analyses were evaluated by nonparametric Kruskal−Wallis test ($n = 3$). ANOVA and Tukey's posthoc test were used in the analyses of the differences between the same PM doses. Differences were considered to be statistically significant at $p < 0.05$.

RESULTS

Particle Synthesis. *Gas Phase Reactions.* The measured concentrations of gases before the first dilution are provided in Table 2. Naturally, the solvent combustion resulted mainly in the formation of carbon dioxide and water vapor. Moisture and the level of O_2 and CO_2 remained constant during and the experiments indicating that the conditions were highly stable. In high-temperature reactions, nitrogen dissociates thermally, oxidizes, and forms nitrogen oxide compounds (NO_x). The average concentration of NO_x varied between 300 and 400 ppm, and was mainly nitrogen monoxide (NO) with a minor fraction of nitrogen dioxide (NO_2). The concentration of CO remained insignificant, although it was slightly elevated during the potassium precursor combustion. This demonstrates that

dx.doi.org/10.1021/tx500142f | Chem. Res. Toxicol. XXXX, XXX, XXX−XXX

the combustion was complete. Moreover, the sulfur dioxide (SO_2) concentrations were on average 110−140 ppm during the combustion of the sulfur-containing precursors (experiments "K/S" and "K/S/Z") and neglible in other cases. These observations indicate that sulfates are most likely the primary component found from the particle phase of "K/S" and "K/S/Zn" experiments.

Particulate Phase. The diameter of the particles produced with the FSP varied between 27 and 45 nm and the number concentration between 5 and 9 × 10^7 cm^{-3}, as determined using the FMPS (Table 4). The analyzed chemical composition of the synthesized particles is provided in Table 5.

Table 4. Crystalline Composition of the PM_1 Samples, Determined by the XRD, and Characteristic Physical Properties of the PM_1

experiment	XRD main components detected	PM_1 (mg m^{-3})	gmd ± std (nm)	gsd (nm)	N_{tot} (cm^{-3} × 10^7)
K	$K_{2-x}H_xCO_3$ ($0 < x < 1$)	44.7	26.9 ± 1.2	1.6	9.0 ± 0.7
K/S	$K_{2-x}H_xSO_4$ ($0 < x < 1$)	109.7	44.5 ± 1.9	1.4	5.1 ± 0.4
K/S/Zn	$K_{2-x}H_xSO_4$ ($0 < x < 1$)	82.2	40.5 ± 3.0	1.4	5.4 ± 1.2
Zn	ZnO	85.2	34.8 ± 1.3	1.6	5.8 ± 0.3

The "K" synthesis produced a high number of small particles (Table 4). In the TEM samples, only agglomerated groups of particles were observed (Figure 2a). The main end product was confirmed as K_2CO_3 by the XRD (Table 4). However, in comparison to other samples relatively high amounts of particulate nitrate ions were determined by the IC (Table 5). This indicates the presence of KNO_3, which is typically formed from potassium reactions with gaseous nitric acid and is a common secondary atmospheric aerosol derived from biomass burning.[47]

According to structural characterization (Table 4), combustion of the "Zn" precursor produced pure ZnO nanoparticles. Gaseous zinc exists only in relatively high temperature and in reducing atmosphere. In an oxidative environment, the zinc oxidizes to ZnO, which instead has very low vapor pressure leading to instant phase transition from gas to solid ZnO. The produced ZnO particles were phase pure, single crystalline, and rod-shaped (Figure 2c), similar to pure ZnO nanorods produced by Height et al.[46] at similar conditions. The crystallite size of ZnO rods was 56 nm and the crystal aspect ratio 2.8. The morphology of the particles indicates wurtzite phase with growth orientation [001].[48]

The experiments using "K/S" and "K/S/Zn" precursors produced particles that composed mainly of sulfates (SO_4^{2-}, 55−65%) and potassium (K, 20%), according to the ICP-MS and IC. The XRD suggested that the main product of the "K/S" and "K/S/Zn" experiments were potassium sulfate or potassium bisulfate (Table 4). Moreover, it is known that sulfuric acid (H_2SO_4) forms readily in humid conditions with water vapor. A known dissociation reaction of H_2SO_4(aq) also produces bisulfate and sulfate ions. On the basis of low K/SO_4^{2-} ratios found at ICP-MS and IC analyses, the sulfate particles are most likely composed partly of H_2SO_4 and water.[49] This was supported by the observation that the particles appeared porous in TEM (Figure 2b and d), unlike the particles in "K" and "Zn". The electron irradiation increases the target temperature, thereby easing the dissociation or sublimation of the species, especially at the extremely low operating pressure (below 10^{-4} Pa) used in TEM. Thus, the porosity of particles may indicate a different phase equilibrium for different sulfates and water in TEM. Finally, the analyzed mass fraction of zinc in "K/S/Zn" particles was 0.8% (ICP-MS). Particulate ZnO was not detected inside sulfate particles (Figure 2d), and zinc was also barely detectable by EDS. The observations lead to the conclusion that the end products of both experiments had similar composition, potassium sulfate and bisulfate being the main end products.

Thermodynamic Equilibrium Calculations. The equilibrium calculations support the findings above. First, the results for "Zn" were straightforward. At the experimental conditions, the predicted transformation temperature of gaseous zinc to solid ZnO was around 1350 °C. Further conclusion of this was that the formation of solid ZnO took place instantly as the vapor encountered oxidizing conditions, at the latest by entering the flow reactor tube.

Second, K_2CO_3 was predicted to be the most probable solid compound produced in the "K" reaction. According to calculations, the KOH vapor reacts with CO_2 to form solid potassium carbonate (K_2CO_3), as the gas temperature approached 900 °C. However, also solid potassium nitrate KNO_3 was suggested to form below 300 °C. That would be a reasonable source of nitrate ions detected by the IC (Table 5).

Third, in the sulfur rich reactions "K/S" and "K/S/Zn", the gaseous KOH was most likely to react with SO_2 to form potassium sulfate (K_2SO_4). A transformation temperature of approximately 1000 °C was predicted for the formation of solid K_2SO_4. Also, liquid sulfuric acid (H_2SO_4), as a hydrate, was in phase equilibrium with gases and solid K_2SO_4, as the temperature reached below 130 °C, supporting the analyses.

Finally, the fate of zinc in the reaction "K/S/Zn" was assessed. According to equilibrium, the existence of both solid ZnO and solid $ZnSO_4$ was suggested at temperatures of 1300 and 630 °C, respectively. In the atmosphere, $ZnSO_4 \cdot H_2O$ may arise as a secondary sulfate from the reaction of zinc oxide with sulfuric acid;[50] however, in the current study it was not detected in the XRD. The relatively low conversion temper-

Table 5. Central Ash Forming Elements and Anions Analyzed from the Particulate Samples with ICP-MS and IC[a]

experiment	K (ng mg^{-1})	Zn (ng mg^{-1})	SO_4^{2-} (ng mg^{-1})	NO_3^- (ng mg^{-1})	Na (ng mg^{-1})	Cl (ng mg^{-1})	other t.m. (ng mg^{-1})
K	420 000	9 00	50 900	26 500	4 000	1 400	700
Zn	4 000	560 000	44 600	BDL	2 000	1 400	300
K/S/Zn	182 000	8 400	550 000	BDL	6 000	1 140	1 100
K/S	220 000	1 900	648 000	1 300	4 000	2 400	1 000
wood PM	300 000	58 000	217 000	2 660	18 000	154 000	14 400

[a]Other t.m. = other transition metals: Cd, Cr, Cu, Fe, Mn, Pb, and Mo. BDL = below detection limit. The wood combustion PM data were adopted from Uski et al.[17].

dx.doi.org/10.1021/tx500142f | *Chem. Res. Toxicol.* XXXX, XXX, XXX−XXX

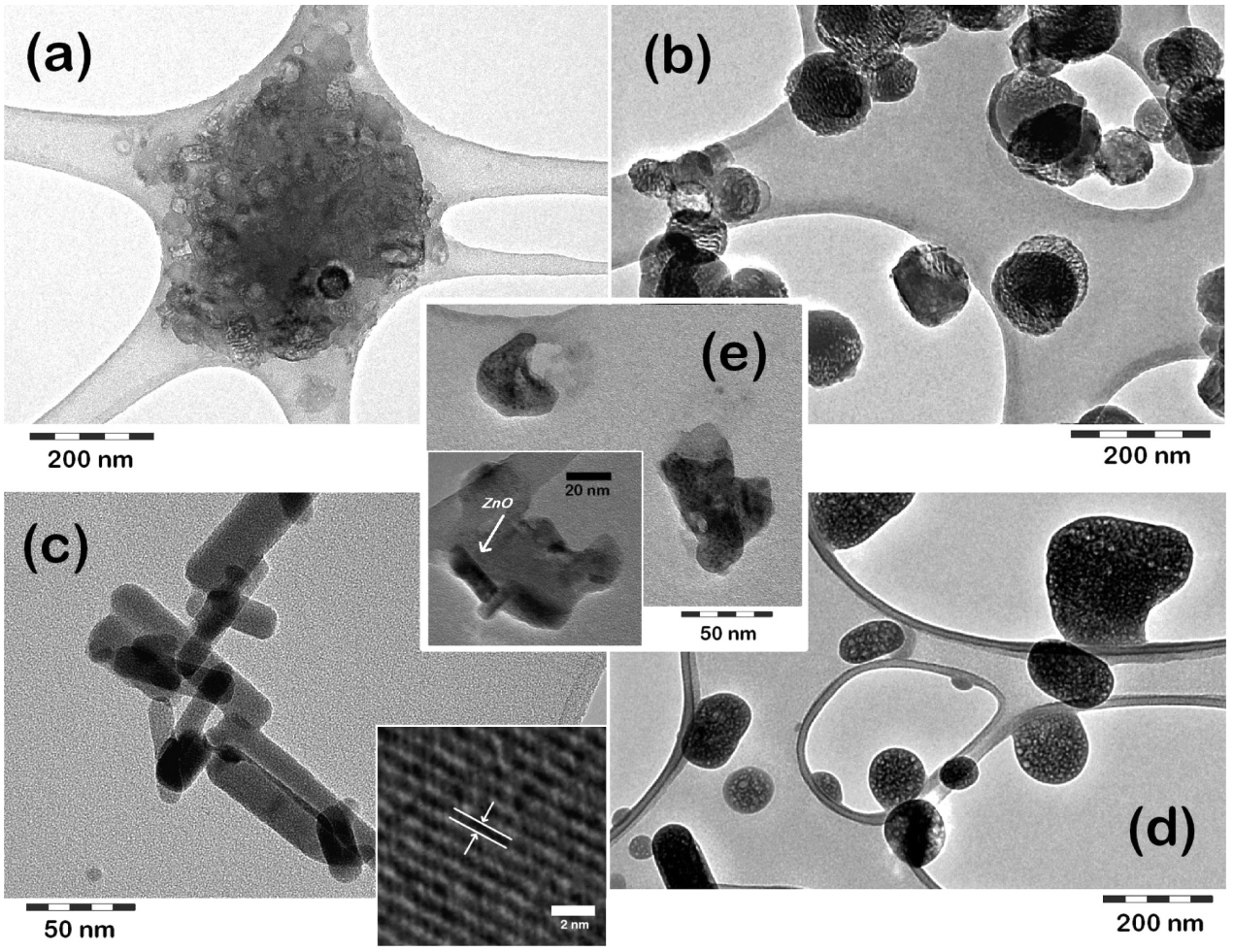

Figure 2. TEM images of particles synthesized with the FSP (a–d) and particles from wood combustion (e). Shown are the K_2CO_3 (a), K_2SO_4 (b), ZnO (c), and K_2SO_4 + Zn (d) composite particles. Inset in c: lattice fringe spacing of 2.5 ± 0.2 Å for the ZnO (002) lattice plane was determined. Inset in e: the white arrow shows an example of a large, rod-shaped ZnO nucleus located in an ash particle formed in efficient wood combustion. Most of the ZnO nuclei were smaller and more evenly distributed inside the cover, which is composed mainly of inorganic species.

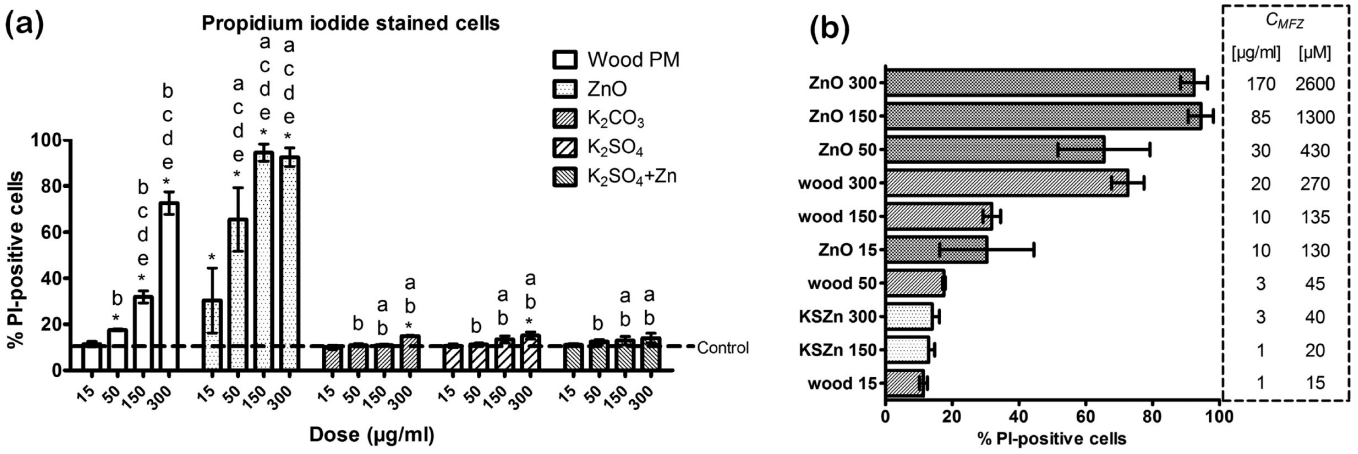

Figure 3. Acute cytotoxicity of particulate samples in RAW264.7 macrophages cells: (a) RAW264.7 macrophages were exposed for 24 h to the PM samples. Cytotoxicity was evaluated using the propidium iodide (PI) exclusion test (n = 3). Corresponding DMSO concentrations were 4.2, 14.0, 41.1, and 84.2 μM, and H_2O concentrations were 0.2, 0.6, 1.7, and 3.3 mM in the exposure medium. Each whisker represents the standard error of the mean (SEM). The asterisks indicate statistical significance compared to the blank substrate control ($p < 0.05$) analyzed by the nonparametric Kruskal–Wallis test. The letters indicate a statistically significant response to the PM samples ($p < 0.05$) based on ANOVA and Tukey's test. a, wood PM; b, ZnO; c, K_2CO_3; d, K_2SO_4; and e, K_2SO_4 + Zn. (b) Illustration of the correspondence of the PI exlusion test response and maximum free zinc ion concentration (C_{MFZ} in μg mL^{-1} or μM) in cell culture medium.

dx.doi.org/10.1021/tx500142f | Chem. Res. Toxicol. XXXX, XXX, XXX–XXX

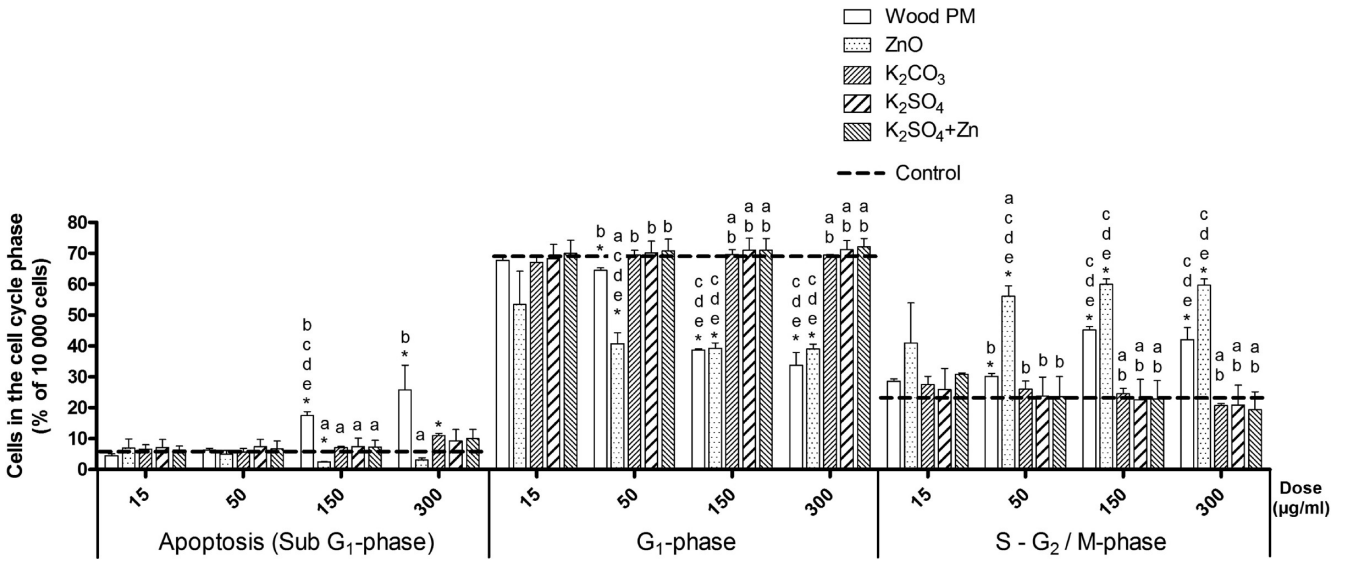

Figure 4. Percentages of mouse RAW264.7 macrophages in the different phases of the cell cycle (SubG_1, G_1, and S-G_2/M) after exposure to different concentrations (15, 50, 150, and 300 mg mL^{-1}) of emission particles from different combustion situations. Corresponding DMSO concentrations were 4.2, 14.0, 41.1, and 84.2 μM, and H_2O concentrations were 0.2, 0.6, 1.7, and 3.3 mM in the exposure medium. The asterisks indicate statistical significance compared to the blank substrate control ($p < 0.05$) analyzed by a nonparametric Kruskal–Wallis test. The letters indicate statistically larger responses ($p < 0.05$) by ANOVA and Tukey's test compared to those of other PM samples. a, wood PM; b, ZnO; c, K_2CO_3; d, K_2SO_4; and e, K_2SO_4 + Zn.

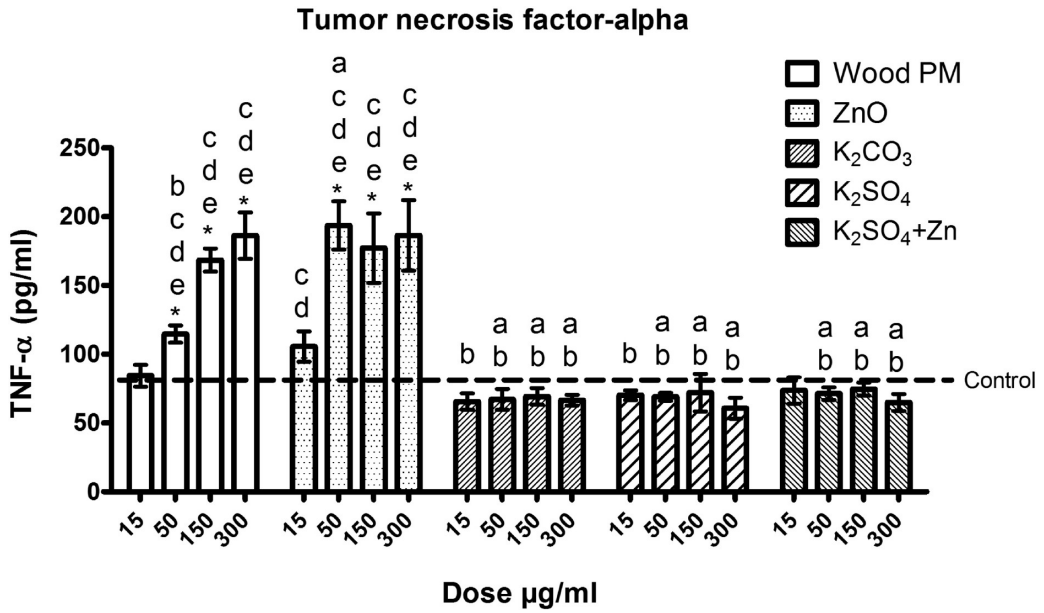

Figure 5. Concentrations of tumor necrosis factor alpha (TNF-α) (pg mL^{-1}) after 24 h exposure of the RAW264.7 macrophages to PM_1 samples. Corresponding DMSO concentrations were 4.2, 14.0, 41.1, and 84.2 μM, and H_2O concentrations were 0.2, 0.6, 1.7, and 3.3 mM in the exposure medium. Bars represent four concentrations (15, 50, 150, and 300 mg mL^{-1}); whiskers are the standard error of the mean (SEM). The asterisks indicate statistical significance compared to the blank substrate control ($p < 0.05$) by ANOVA and Dunnett's test. The letters indicate a statistically larger response ($p < 0.05$) by ANOVA and Tukey's test compared to that of the other PM samples. a, wood PM; b, ZnO; c, K_2CO_3; d, K_2SO_4; e, K_2SO_4 + Zn.

atures calculated for solid potassium and sulfur species indicate that they do not yet exist at high flame temperatures of FSP but rather at the flow reactor tube. However, in the mixed precursor "K/S/Zn" combustion there is a possibility that the high concentration vapor phase sulfur species already influence the early cluster formation of ZnO.[46]

Comparison to Wood Combustion PM. In comparison with the wood combustion, PM similarities in the chemical composition and morphology were found with the synthesized counterparts. The concentrations and size of the particles correspond well with particles formed in combustion of the wood chip[14] used as a comparison in this study. A detailed morphological and chemical analysis of the wood combustion particles was recently reported by Torvela et al.[51] According to the study, the particles were composed mainly of alkali metal salts (approximately 67% of PM_1). Up to approximately 40% of the PM_1 was potassium sulfate (sulfate ions 22% of PM_1). Zinc concentration was approximately 6% of the PM_1. Zinc was

dx.doi.org/10.1021/tx500142f | *Chem. Res. Toxicol.* XXXX, XXX, XXX–XXX

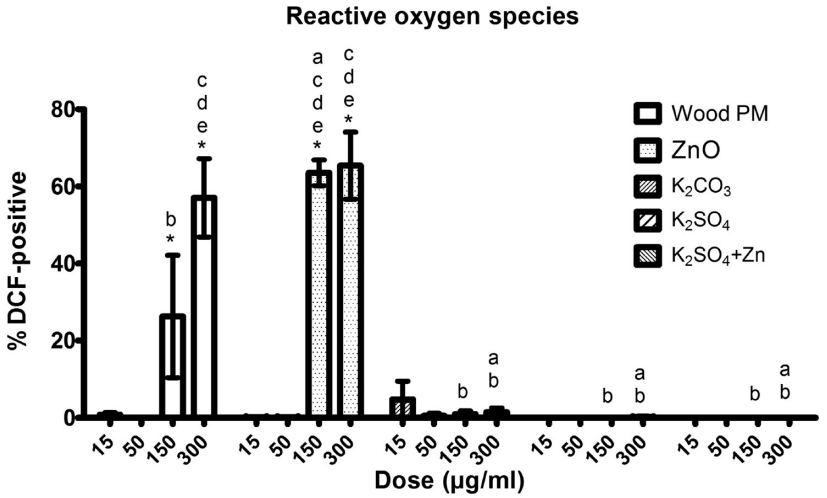

Figure 6. Formation of reactive oxygen species (percentage of DCF+ cells ± SEM) in RAW264.7 macrophages after exposure to four concentrations (15, 50, 150, and 300 mg mL^{-1}) of the PM_1 samples from different combustion situations. Corresponding DMSO concentrations were 4.2, 14.0, 41.1, and 84.2 μM, and H_2O concentrations were 0.2, 0.6, 1.7, and 3.3 mM in the exposure medium. The asterisks indicate statistical significance compared to the blank substrate control ($p < 0.05$) analyzed by nonparametric Kruskal–Wallis test. The letters indicate statistically larger responses ($p < 0.05$) in ANOVA and Tukey's test compared to those of the other PM samples. a, wood PM; b, ZnO; c, K_2CO_3; d, K_2SO_4; and e, K_2SO_4 + Zn.

found as ZnO crystals, with diameter below 13 nm, inside the alkali salt core. The particles contained also minor amounts of other transition metals, such as cromium, manganese, and lead (Table 5). The fraction of organic and elemental carbon was below 3% of the PM_1, due to the high efficiency of the combustion process. The geometric mean diameter of particles was 50 nm. A TEM image of the particles is shown in Figure 2e.

Toxicological Responses to Particulate Samples. In the following toxicological analysis report, the particles are denoted as ZnO (Figure 2c), K_2SO_4 (Figure 2b), K_2SO_4 + Zn (Figure 2d), K_2CO_3 (Figure 2a), and wood combustion PM (Figure 2e), according to the main chemical species analyzed for the samples. Wood combustion PM physicochemical data and toxicity are adopted from an earlier report by Uski et al.[17] All toxicological analyses were done with the mouse macrophage cell line, which provides a model to study the mechanisms activated in the cells of the first line immune defense against particles in lungs.

Cytotoxicity. Figure 3a shows the acute cytotoxicity in RAW 264.7 macrophage cells as assayed with a PI exclusion assay. At the lowest dose (15 μg mL^{-1}), the only sample inducing statistically significant cell death was the ZnO particles. At higher doses, the exposure for ZnO lead to rapid decrease in cell viability, showing a saturation point at the second highest dose (150 μg mL^{-1}). The exposure to wood combustion PM showed a similar intense decrease of cell viability but with particle mass based doses that were 3–6 times higher than those with exposure to ZnO. However, when the instilled dose is expressed as the maximum free zinc ion concentration (C_{MFZ}, Figure 3b) the dose–response is similar for both samples. The acute cytotoxic effects onset (exceed 50%) at C_{MFZ} between 10 and 30 μg mL^{-1} (130–430 μM). The acute cytotoxic effects of synthetic K_2CO_3 and K_2SO_4 particles were only a few percent over the control level at the highest dose. The K_2SO_4 + Zn particles did not induce any cytotoxic effects; however, further conclusions on the cytotoxicity of "K/S/Zn" samples could not be made; at the two highest doses (150 and 300 μg mL^{-1}), the C_{MFZ} (20–40 μM Zn^{2+}) was below the 50% effective level as can be seen in Figure 3b.

Cell Cycle Analysis. Figure 4 shows the results of the cell cycle analysis. An accumulation of cells in the S/G_2 phase was observed for both wood combustion PM and synthetic ZnO. Other particulate samples did not intrude the cell cycle compared to the control. In addition, wood combustion PM evoked significantly increased apoptotic response at the two highest doses.

Inflammation and ROS Production. The TNF-α production after 24-h exposure of macrophages is shown in Figure 5. Only wood combustion PM and ZnO were observed to induce a significant TNF-α production in the cells. In addition, a clear generation of ROS was detected after the exposure of RAW 264.7 macrophages to PM from wood combustion and ZnO synthesis (Figure 6) at particle mass doses of 150 and 300 mg mL^{-1}. Other samples had no effect on inflammation or ROS responses.

DISCUSSION

In this study, it was shown that efficient wood combustion PM evoked acute cytotoxicity, cell cycle arrest, ROS generation, and TNF-α release in mouse magrophage cells, with a profile similar to that of pure ZnO particles. The ZnO nanoparticles showed more intense toxicity in almost all measured end points when particle mass was used as the dose metric. However, for both ZnO and wood combustion PM, the acute cytotoxicity was found to be similarly dose-dependent on the maximum free zinc ion concentration of particulate samples and was onset typically at C_{MFZ} of 10–30 μg mL^{-1} (130–450 μM). At the same time, potassium carbonates and sulfates, which are major components of wood combustion PM and secondary aerosols found in ambient air, were found not to induce toxic effects even at high doses.

The physicochemical analysis of the particle samples as well as analysis of the combustion gases and calculations confirmed that the synthesized particles were composed mainly of potassium carbonate and nitrate, potassium sulfates, or of zinc oxide. The physical size and appearance of the synthesized particles were comparable to some specific features observed in wood combustion generated PM. In contrast to the

dx.doi.org/10.1021/tx500142f | Chem. Res. Toxicol. XXXX, XXX, XXX–XXX

manufactured counterparts, composition of the combustion derived particles was more complex. The possibility of coexisting species having unknown interactions with biological systems makes it difficult to derive causal links between the physical properties of particles and the shown experimental outcomes.[35] However, in light of the results in the present study, the toxic potential of zinc in wood combustion PM seems to remain despite the coexisting species.

Only apoptosis was more enhanced in wood combustion PM than in ZnO nanoparticles. The wood combustion particles were found to contain less than 3% of carbonaceous material. The known toxicity of OC could be the factor behind the apoptotic behavior of magrophage cells in response to the increasing particulate mass of combustion generated particles. However, the various transition metals other than zinc, absent in the synthetic particles, could be the more relevant factors in this case. For instance, chromium is a well-known inducer of apoptotic cell death.[52]

Previously, zinc sulfate has been reported to induce cell cycle G_2 arrest with human alveolar epithelial cells (A549).[53] In addition, Wong et al.[54] demonstrated that zinc ions induced G_2/M cell cycle arrest in human bronchial epithelial cells. Also, DNA damage may cause cell cycle delays or arrests since damaged DNA may stop the cells from passing through various checkpoints in the cell cycle.[55] Thus, oxidative DNA damage induced by zinc is a possible mechanism for the cell cycle effects observed in the present study. The findings on cytotoxicity and TNF-α release agree with the results of previous *in vivo* studies, which indicated that particles from near-complete wood combustion are more potent inducers of tissue damage and inflammation than those emitted from more incomplete combustion processes.[15,16]

The observations are also in line with other previous studies. Wang et al.[56] and Zhang et al.[57] have shown that the oxidative stress potential of ambient PM significantly correlates with the Zn content of the PM. In a study by Tsou et al.,[58] human promonocyte cell line was exposed to Zn^{2+}, which lead to significant releases of inflammatory cytokines, including IL-6, IL-7, IL-8, and IL-10. Moreover, Xia et al.[18] detected significant IL-8 release from BEAS-2B cells and TNF-α response from RAW274.7 cells after exposure to ZnO NPs. When the cell's antioxidant defense mechanisms fail to protect against cellular injury, the proinflammatory cascades are activated. The Jun kinase (JNK) and NF-$\kappa\beta$ cascades are redox sensitive signaling cascades that are capable of inducing the expression of proinflammatory cytokines and chemokines, e.g., TNF-α.[35,59] In addition, zinc nanoparticles (NP) have been reported to evoke the formation of ROS,[60] as was also observed in this study.

Although Zn^{2+} ions are thought to be behind toxic effects, it has been shown *in vitro* that also ZnO particles may induce toxic reactions without a significant free ion release rate in the medium.[18,22,61] It is, however, under discussion whether a direct contact to cells is required[21] to induce those effects and which pathways are activated by the particulate zinc. ZnO is able to dissolve in tissue culture media to release zinc ions, but a major conclusion of previous research[18,62] is that ZnO nanoparticles are internalized into cells prior to dissolution. For instance, Sotiriou et al.[62] detected ZnO nanoparticle mediated DNA damage already at 4 h incubation times, which did not precede sufficient ZnO dissolution into the RPMI cell culture medium.

Overall, the cell culture medium is playing a key role due to dissolved salts and proteins, which for instance increase the dissolution rate of metal oxides.[63] Xia et al.[18] determined 190−225 μM as the maximum total dissolved zinc for ZnO nanoparticles into two different cell culture media. On the contrary, Sotiriou et al.[62] did not find equilibrium for flame spray made ZnO nanoparticle dissolution kinetics in RPMI after 24 h, with particle mass dose of 100 μg mL^{-1} which corresponds well with this study. The overall dissolution of ZnO according to that study was approximately 50% in RPMI, which is high among other metal oxide nanoparticles, whose electron transfer properties seem to play a higher role in their cytotoxicity than ion release by dissolution.[64] Moreover, it has been shown[18,64,65] that flame made ZnO particle hydrodynamic size submerged in tissue culture media differs from that of primary particle size, which is a plausible scenario also in the current article. On the basis of the results above, the highest doses of ZnO NPs in this study (C_{MFZ} 430−2600 μM) most likely remained partially in particulate form, but the dissolution on ZnO in submerged conditions plays a central role in the observed toxicity. It is not known whether the zinc in wood combustion PM (14−250 μM) follows the same dissolution kinetics as ZnO nanoparticles, as the alkali salt shell was covering the ZnO cores of the wood PM. However, the observations made in this study indicate that the shell, proved as nontoxic itself, did not prevent cell contact with the toxic ZnO cores.

In this study, application of suspended particulate matter in cell medium was used to achieve the delivery of combustion particle samples to the cell attached to the bottom of the well. Important issues to be considered are the sample treatment after the filter collection and specifically how the samples were extracted from the filters. The multiple extraction and suspension steps of the procedure change, at least to some extent, the properties of the particles, and it is probable that the particles do not occur in their original size in the cell culture medium. Moreover, when the methanol particulate suspension is evaporated from the sample tubes, the particles become attached to the tubes. Therefore, a slight amount of DMSO is needed during the suspension of particulate samples to detach the samples from the tubes. This treatment also probably causes changes in PM size, surface properties, and solubility. However, DMSO is widely used in *in vitro* and *in vivo* studies because of its ability to dissolve and disperse hydrophobic and hydrophilic substances and particles. DMSO can also easily penetrate through biological membranes and cellular barriers.[66] Therefore, it is possible that the transportation of particles through the cell membrane may be enhanced. In addition, known inflammatory, anti-inflammatory, and ROS scavenging properties of DMSO[66] were excluded in pilot studies which showed no difference in any measured parameters (data not shown).

The current study shows that the parallel cytotoxic behavior of the complete wood combustion PM and particulate ZnO is connected partly, but not completely, to the maximum free zinc ion concentration. This does not rule out the possibility of particle mediated toxic effects. As a conclusion, it was shown that the toxic potential of efficient wood combustion PM is likely caused by specific metal species such as zinc, when the mass of carbonaceous species in the PM is minor. Therefore, more attention should be paid to the contents of volatile transition metals in biomass fuels.

AUTHOR INFORMATION

Corresponding Author

*Phone: +358 40 3553123. Fax: +358 17 163098. E-mail: tiina.torvela@uef.fi.

Funding

This study was funded by the Finnish Funding Agency of Technology and Innovation (Tekes ERA-NET Bioenergy; 40392/09) and the Research Programme on Sustainable Energy of the Academy of Finland. This project belongs to the strategic funding of the University of Eastern Finland (Sustainable Bioenergy, Climate Change and Health).

Notes

The authors declare no competing financial interest.

ACKNOWLEDGMENTS

We thank Terhi Kaivosoja, Miia Koistinen, Valtteri Suonmaa, and Annika Virén for participation in the laboratory work and analyses and Sirpa Peräniemi for special assistance with particulate sample analyses.

ABBREVIATIONS

C_{MFZ}, maximum free zinc ion concentration; CPC, condensation particle counter; DCF, dichlorofluorescein assay; DGI, Dekati gravimetric impactor; DMSO, dimethyl sulfoxide C_2H_6OS; DR, dilution ratio; EC, elemental carbon; ED, ejector diluter; EDS, energy dispersive X-ray spectrometry; FMPS, fast mobility particle sizer; FSP, flame spray pyrolysis; FTIR, Fourier transform infrared analyzer; IC, ion chromatography; ICP-MS, inductively coupled plasma mass spectrometer; LDH, lactate dehydrogenase; OC, organic carbon; PBS, phosphate buffered saline; PI, propidium iodide; PM_i, particulate mass, mass of particles less than i μm in aerodynamic diameter; PRD, porous tube diluter; PTFE, polytetrafluoroethylene (Teflon); ROS, reactive oxygen species; RPMI, Roswell Park Memorial Institute cell culture medium; TEM, transmission electron microscopy; TNF-α, tumor necrosis factor alpha; UFP, ultrafine particles, particles less than 100 nm in aerodynamic diameter; XRD, X-ray diffraction

REFERENCES

(1) World Health Organization (2004) *Health Aspects of Air Pollution. Results from the Project "Systematic Review of Health Aspects of Air Pollution in Europe"*, World Health Organization, Copenhagen, Denmark.

(2) Brook, R. D., Rajagopalan, S., Pope, C. A., Brook, J. R., Bhatnagar, A., Diez-Roux, A. V., Holguin, F., Hong, Y., Luepker, R. V., Mittleman, M. A., Peters, A., Siscovick, D., Smith, S. C., Whitsel, L., and Kaufman, J. D. (2010) Particulate matter air pollution and cardiovascular disease: an update to the scientific statement from the American Heart Association. *Circulation 121*, 2331−2378.

(3) Hellén, H., Hakola, H., Haaparanta, S., Pietarila, H., and Kauhaniemi, M. (2008) Influence of residential wood combustion on local air quality. *Sci. Total Environ. 393*, 283−290.

(4) Burnett, R. T., Brook, J., Dann, T., Delocla, C., Philips, O., Cakmak, S., Vincent, R., Goldberg, M. S., and Krewski, D. (2000) Association between particulate- and gas-phase components of urban air pollution and daily mortality in eight canadian cities. *Inhalation Toxicol. 12*, 15−39.

(5) Tissari, J., Lyyränen, J., Hytönen, K., Sippula, O., Tapper, U., Frey, A., Saarnio, K., Pennanen, A., Hillamo, R., Salonen, R., Hirvonen, M.-R., and Jokiniemi, J. (2008) Fine particle and gaseous emissions from normal and smouldering wood combustion fired in a conventional masonry heater. *Atmos. Environ. 42*, 7862−7873.

(6) Schwarze, P. E., Ovrevik, J., Lag, M., Refsnes, M., Nafstad, P., Hetland, R. B., and Dybing, E. (2006) Particulate matter properties and health effects: consistency of epidemiological and toxicological studies. *Hum. Exp. Toxicol. 25*, 559−579.

(7) Wu, W., Bromberg, P., and Samet, J. (2013) Zinc ions as effectors of environmental oxidative lung injury. *Free Radical Biol. Med. 65*, 57−69.

(8) Bäfver, L., Leckner, B., Tullin, C., and Berntsen, M. (2011) Particle emissions from pellets stoves and modern and old-type wood stoves. *Biomass Bioenergy 35*, 3648−3655.

(9) Lippmann, M., Yeates, D., and Albert, R. (1980) Deposition, retention, and clearance of inhaled particles. *Br. J. Ind. Med. 37*, 337−362.

(10) Kreyling, W. G., Semmler-Behnke, M., and Möller, W. (2006) Ultrafine particle-lung interactions: does size matter? *J. Aerosol Med. 19*, 74−83.

(11) Delfino, R., Sioutas, C., and Malik, S. (2005) Potential role of ultrafine particles in associations between airborne particle mass and cardiovascular health. *Environ. Health Perspect. 113*, 934−946.

(12) Sioutas, C., Delfino, R., and Singh, M. (2005) Exposure assessment for atmospheric ultrafine particles (UFPs) and implications in epidemiologic research. *Environ. Health Perspect. 113*, 947−955.

(13) Sippula, O., Hytönen, K., Tissari, J., Raunemaa, T., and Jokiniemi, J. (2007) Effect of wood fuel on the emissions from a top-feed pellet stove. *Energy Fuels 21*, 1151−1160.

(14) Leskinen, J., Tissari, J., Uski, O., Virén, A., Torvela, T., Kaivosoja, T., Lamberg, H., Nuutinen, I., Kettunen, T., Joutsensaari, J., Jalava, P., Sippula, O., Hirvonen, M., and Jokiniemi, J. (2014) Fine particle emissions in three different combustion conditions of a wood chip-fired appliance − Particulate physico-chemical properties and induced cell death. *Atmos. Environ. 86*, 129−139.

(15) Happo, M. S., Uski, O., Jalava, P. I., Kelz, J., Brunner, T., Hakulinen, P., Mäki-Paakkanen, J., Kosma, V.-M., Jokiniemi, J., Obernberger, I., and Hirvonen, M.-R. (2013) Pulmonary inflammation and tissue damage in the mouse lung after exposure to PM samples from biomass heating appliances of old and modern technologies. *Sci. Total Environ. 443*, 256−266.

(16) Uski, O. J., Happo, M. S., Jalava, P. I., Brunner, T., Kelz, J., Obernberger, I., Jokiniemi, J., and Hirvonen, M.-R. (2012) Acute systemic and lung inflammation in C57Bl/6J mice after intratracheal aspiration of particulate matter from small-scale biomass combustion appliances based on old and modern technologies. *Inhalation Toxicol. 24*, 952−965.

(17) Uski, O., Jalava, P., Happo, M., Leskinen, J., Sippula, O., Tissari, J., Mäki-Paakkanen, J., Jokiniemi, J., and Hirvonen, M.-R. (2014) Different toxic mechanisms are activated by emission PM depending on combustion efficiency. *Atmos. Environ. 89*, 623−632.

(18) Xia, T., Kovochich, M., Liong, M., Mädler, L., Gilbert, B., Shi, H., Yeh, J., Zink, J., and Nel, A. (2008) Comparison of the mechanism of toxicity of zinc oxide and cerium oxide nanoparticles based on dissolution and oxidative stress properties. *ACS Nano 2*, 2121−2134.

(19) Adamson, I., Prieditis, H., Hedgecock, C., and Vincent, R. (2000) Zinc is the toxic factor in the lung response to an atmospheric particulate sample. *Toxicol. Appl. Pharmacol. 166*, 111−119.

(20) Walther, U., Czermak, A., Mückter, H., Walther, S., and Fichtl, B. (2003) Decreased GSSG reductase activity enhances cellular zinc toxicity in three human lung cell lines. *Arch. Toxicol. 77*, 131−137.

(21) Moos, P., Chung, K., Woessner, D., Honeggar, M., Cutler, N., and Veranth, J. (2010) ZnO particulate matter requires cell contact for toxicity in human colon cancer cells. *Chem. Res. Toxicol. 23*, 733−739.

(22) Hsiao, I., and Huang, Y. (2011) Effects of various physicochemical characteristics on the toxicities of ZnO and TiO nanoparticles toward human lung epithelial cells. *Sci. Total Environ. 409*, 1219−1228.

(23) Elliott, P., Shaddick, G., Wakefield, J., de Hoogh, C., and Briggs, D. (2007) Long-term associations of outdoor air pollution with mortality in Great Britain. *Thorax 62*, 1088−1094.

(24) Willis, A., Jerrett, M., Burnett, R., and Krewski, D. (2003) The association between sulfate air pollution and mortality at the county

scale: an exploration of the impact of scale on a long-term exposure study. *J. Toxicol. Environ. Health, Part A 66*, 1605−1624.
(25) Abrahamowicz, M., Schopflocher, T., Leffondré, K., du Berger, R., and Krewski, D. (2003) Flexible modeling of exposure-response relationship between long-term average levels of particulate air pollution and mortality in the American Cancer Society study. *J. Toxicol. Environ. Health, Part A 66*, 1625−1654.
(26) Schlesinger, R. (2007) The health impact of common inorganic components of fine particulate matter (PM2.5) in ambient air: a critical review. *Inhalation Toxicol. 19*, 811−832.
(27) Sippula, O., Koponen, T., and Jokiniemi, J. (2012) Behavior of alkali metal aerosol in a high-temperature porous tube sampling probe. *Aerosol Sci. Technol. 46*, 1151−1162.
(28) Jalava, P., Hirvonen, M.-R., Sillanpää, M., Pennanen, A., Happo, M., Hillamo, R., Cassee, F., Gerlofs-Nijland, M., Borm, P. J., Schins, R., Janssen, N., and Salonen, R. (2009) Associations of urban air particulate composition with inflammatory and cytotoxic responses in RAW 246.7 cell line. *Inhalation Toxicol. 21*, 994−1006.
(29) Steerenberg, P. A., van Amelsvoort, L., Lovik, M., Hetland, R. B., Alberg, T., Halatek, T., Bloemen, H. J. T., Rydzynski, K., Swaen, G., Schwarze, P., Dybing, E., and Cassee, F. R. (2006) Relation between sources of particulate air pollution and biological effect parameters in samples from four european cities: an exploratory study. *Inhalation Toxicol. 18*, 333−346.
(30) Jalava, P. I., Salonen, R. O., Nuutinen, K., Pennanen, A. S., Happo, M. S., Tissari, J., Frey, A., Hillamo, R., Jokiniemi, J., and Hirvonen, M.-R. (2010) Effect of combustion condition on cytotoxic and inflammatory activity of residential wood combustion particles. *Atmos. Environ. 44*, 1691−1698.
(31) Jalava, P. I., Happo, M. S., Kelz, J., Brunner, T., Hakulinen, P., Mäki-Paakkanen, J., Hukkanen, A., Jokiniemi, J., Obernberger, I., and Hirvonen, M. (2012) In vitro toxicological characterization of particulate emissions from residential biomass heating systems based on old and new technologies. *Atmos. Environ. 50*, 24−35.
(32) Tapanainen, M., Jalava, P. I., Mäki-Paakkanen, J., Hakulinen, P., Happo, M. S., Lamberg, H., Ruusunen, J., Tissari, J., Nuutinen, K., Yli-Pirilä, P., Hillamo, R., Salonen, R. O., Jokiniemi, J., and Hirvonen, M. (2011) In vitro immunotoxic and genotoxic activities of particles emitted from two different small-scale wood combustion appliances. *Atmos. Environ. 45*, 7546−7554.
(33) Tapanainen, M., Jalava, P. I., Mäki-Paakkanen, J., Hakulinen, P., Lamberg, H., Ruusunen, J., Tissari, J., Jokiniemi, J., and Hirvonen, M.-R. (2012) Efficiency of log wood combustion affects the toxicological and chemical properties of emission particles. *Inhalation Toxicol. 24*, 343−355.
(34) Xia, T., Kovochich, M., Brant, J., Hotze, M., Sempf, J., Oberley, T., Sioutas, C., Yeh, J. I., Wiesner, M. R., and Nel, A. E. (2006) Comparison of the abilities of ambient and manufactured nanoparticles to induce cellular toxicity according to an oxidative stress paradigm. *Nano Lett. 6*, 1794−1807.
(35) Nel, A., Xia, T., Mädler, L., and Li, N. (2006) Toxic potential of materials at the nanolevel. *Science 311*, 622−627.
(36) Mädler, L., Kammler, H., Mueller, R., and Pratsinis, S. (2002) Controlled synthesis of nanostructured particles by flame spray pyrolysis. *J. Aerosol Sci. 33*, 369−389.
(37) Sippula, O., Hokkinen, J., Puustinen, H., Yli-Pirilä, P., and Jokiniemi, J. (2009) Particle emissions from small wood-fired district heating units. *Energy Fuels 23*, 2974−2982.
(38) Tissari, J., Hytönen, K., Lyyränen, J., and Jokiniemi, J. (2007) A novel field measurement method for determining fine particle and gas emissions from residential wood combustion. *Atmos. Environ. 41*, 8330−8344.
(39) Kaivosoja, T., Jalava, P., Lamberg, H., Virén, A., Tapanainen, M., Torvela, T., Tapper, U., Sippula, O., Tissari, J., Hillamo, R., Hirvonen, M., and Jokiniemi, J. (2013) Comparison of emissions and toxicological properties of fine particles from wood and oil boilers in small (20−25 kW) and medium (5−10 MW) scale. *Atmos. Environ. 77*, 193−201.
(40) Lamberg, H., Nuutinen, K., Tissari, J., Ruusunen, J., Yli-Pirilä, P., Sippula, O., Tapanainen, M., Jalava, P., Makkonen, U., Teinilä, K., Saarnio, K., Hillamo, R., Hirvonen, M.-R., and Jokiniemi, J. (2011) Physicochemical characterization of fine particles from small-scale wood combustion. *Atmos. Environ. 45*, 7635−7643.
(41) Ruusunen, J., et al. (2011) A novel particle sampling system for physico-chemical and toxicological characterization of emissions. *Anal. Bioanal. Chem. 401*, 3183−3195.
(42) Jalava, P., Salonen, R. O., Hälinen, A. I., Sillanpää, M., Sandell, E., and Hirvonen, M.-R. (2005) Effects of sample preparation on chemistry, cytotoxicity, and inflammatory responses induced by air particulate matter. *Inhalation Toxicol. 17*, 107−117.
(43) Scherrer, P. (1918) Bestimmung der Größe und der inneren Struktur von Kolloidteilchen mittels Röntgenstrahlen. *Nachr. Ges. Wiss. Goettingen, Math.-Phys. Kl. 1918*, 98−100.
(44) Energy Research Centre of the Netherlands (2014) Database for Biomass and Waste. https://www.ecn.nl/phyllis2.
(45) Bale, C., Chartrand, P., Degterov, S., Eriksson, G., Hack, K., Mahfoud, K., Melancon, J., Pelton, A., and Petersen, S. (2002) Factsage thermochemical software and databases. *Calphad 26*, 189−228.
(46) Height, M., Mädler, L., and Pratsinis, S. (2006) Nanorods of ZnO made by flame spray pyrolysis. *Chem. Mater. 18*, 572−578.
(47) Freney, E. J., Garvie, L. A. J., Groy, T. L., and Buseck, P. R. (2009) Growth and single-crystal refinement of phase-III potassium nitrate, KNO_3. *Acta Crystallogr., Sect. B: Struct. Sci. 65*, 659−663.
(48) Ge, M., Wu, H., Niu, L., Liu, J., Chen, S., Shen, P., Zeng, Y., Wang, Y., Zhang, G., and Jiang, J. (2007) Nanostructured ZnO: From monodisperse nanoparticles to nanorods. *J. Cryst. Growth 305*, 162−166.
(49) Sippula, O., Hokkinen, J., Puustinen, H., Yli-Pirilä, P., and Jokiniemi, J. (2009) Comparison of particle emissions from small heavy fuel oil and wood-fired boilers. *Atmos. Environ. 43*, 4855−4864.
(50) Biggins, P., and Harrison, R. (1979) Characterization and classification of atmospheric sulfates. *JAPCA 29*, 838−840.
(51) Torvela, T., Tissari, J., Sippula, O., Kaivosoja, T., Leskinen, J., Virén, A., Lähde, A., and Jokiniemi, J. (2014) Effect of wood combustion conditions on the morphology of freshly emitted fine particles. *Atmos. Environ. 87*, 65−76.
(52) Bagchi, D. (2002) Cytotoxicity and oxidative mechanisms of different forms of chromium. *Toxicology 180*, 5−22.
(53) Könczöl, M., Goldenberg, E., Ebeling, S., Schäfer, B., Manuel, G., Gminski, R., Grobéty, B., Barbara, R., Merfort, I., Gieré, R., and Volker, M. (2012) Cellular uptake and toxic effects of fine and ultrafine metal-sulfate particles in human A549 lung epithelial cells. *Chem. Res. Toxicol. 25*, 2687−2703.
(54) Wong, S., Shih, R., Schoene, N., and Lei, K. (2008) Zinc-induced G2/M blockage is p53 and p21 dependent in normal human bronchial epithelial cells. *Am. J. Physiol.: Cell Physiol. 294*, C1342−C1349.
(55) King, K. L., and Cidlowski, J. A. (1998) Cell cycle regulation and apoptosis. *Annu. Rev. Physiol. 60*, 601−617.
(56) Wang, D., Pakbin, P., Shafer, M. M., Antkiewicz, D., Schauer, J. J., and Sioutas, C. (2013) Macrophage reactive oxygen species activity of water-soluble and water-insoluble fractions of ambient coarse, PM2.5 and ultrafine particulate matter (PM) in Los Angeles. *Atmos. Environ. 77*, 301−310.
(57) Zhang, Y., Schauer, J. J., Shafer, M. M., Hannigan, M. P., and Dutton, S. J. (2008) Source apportionment of in vitro reactive oxygen species bioassay activity from atmospheric particulate matter. *Environ. Sci. Technol. 42*, 7502−7509.
(58) Tsou, T.-C., Chao, H.-R., Yeh, S.-C., Tsai, F.-Y., and Lin, H.-J. (2011) Zinc induces chemokine and inflammatory cytokine release from human promonocytes. *J. Hazard. Mater. 196*, 335−341.
(59) Warheit, D., Laurence, B., Reed, K., Roach, D., Reynolds, G., and Webb, T. (2004) Comparative pulmonary toxicity assessment of single-wall carbon nanotubes in rats. *Toxicol. Sci. 77*, 117−125.
(60) Sharma, A. D. V., and Dhawan, A. (2012) Zinc oxide nanoparticles induce oxidative DNA damage and ROS-triggered

mitochondria mediated apoptosis in human liver cells (HepG2). *Apoptosis 17*, 852−870.
(61) Shen, C., James, S. A., de Jonge, M. D., Turney, T. W., Wright, P. F. A., and Feltis, B. N. (2013) Relating cytotoxicity, zinc ions, and reactive oxygen in ZnO nanoparticle-exposed human immune cells. *Toxicol. Sci. 136*, 120−130.
(62) Sotiriou, G., Watson, C., Murdaugh, K., Darrah, T., Pyrgiotakis, G., Elder, A., Brain, J., and Demokritou, P. (2014) Engineering safer-by-design silica-coated ZnO nanorods with reduced DNA damage potential. *Environ. Sci.: Nano 1*, 144−153.
(63) Ma, R., Levard, C., Michel, F. M., Brown, G. E., and Lowry, G. V. (2013) Sulfidation mechanism for zinc oxide nanoparticles and the effect of sulfidation on their solubility. *Environ. Sci. Technol. 47*, 2527−2534.
(64) Zhang, H., et al. (2012) Use of metal oxide nanoparticle band gap to develop a predictive paradigm for oxidative stress and acute pulmonary inflammation. *ACS Nano 6*, 4349−4368.
(65) Raemy, D. O., Grass, R. N., Stark, W. J., Schumacher, C. M., Clift, M. J., Gehr, P., and Barbara, R. (2012) Effects of flame made zinc oxide particles in human lung cells - a comparison of aerosol and suspension exposures. *Part. Fibre Toxicol. 9*, 33.
(66) Colucci, M., Maione, F., Bonito, M., Piscopo, A., Di Giannuario, A., and Pieretti, S. (2008) New insights of dimethyl sulfoxide effects (DMSO) on experimental in vivo models of nociception and inflammation. *Pharmacol. Res.*, 419−425.